Relativistic Effects and the Unique Low-Symmetry Structures of Gold Nanoclusters

Wei Huang,[†,‡] Min Ji,[†] Chuan-Ding Dong,[†] Xiao Gu,[†] Lei-Ming Wang,[‡] Xin Gao Gong,[†,]* and Lai-Sheng Wang[‡,§,]*

[†]Surface Physics Laboratory and Department of Physics, Fudan University, Shanghai 200433, China, [‡]Department of Physics, Washington State University, 2710 University Drive, Richland, Washington 99354, and [§]Chemical & Materials Sciences Division, Pacific Northwest National Laboratory, Richland, Washington 99352

ABSTRACT The atomic structures of bare gold clusters provide the foundation to understand the enhanced catalytic properties of supported gold nanoparticles. However, the richness of diverse structures and the strong relativistic effects have posed considerable challenges for a systematic understanding of gold clusters with more than 20 atoms. We use photoelectron spectroscopy of size-selected anions, in combination with first principles calculations, to elucidate the structures of gold nanoclusters in a critical size regime from 55 to 64 atoms (1.1−1.3 nm in diameter). Au_{55}^- is found to be a nonicosahedral disordered cluster as a result of relativistic effects that induce strong surface contractions analogous to bulk surface reconstructions, whereas low-symmetry core−shell-type structures are found for Au_{56}^- to Au_{64}^-. Au_{58} exhibits a major electron-shell closing and is shown to possess a low-symmetry, but nearly spherical structure with a large energy gap. Clear spectroscopic and computational evidence has been observed, showing that Au_{58}^- is a highly robust cluster and additional atoms are simply added to its surface from Au_{59}^- to Au_{64}^- without inducing significant structural changes. The unique low-symmetry structures characteristic of gold nanoclusters due to the strong relativistic effects allow abundant surface defects sites, providing a key structure−function relationship to understand the catalytic capabilities of gold nanoparticles.

KEYWORDS: photoelectron spectroscopy · gold clusters · density functional theory · structure−function relationship · electronic structure

G old is the most inert metal in the periodic table, but at the nanometer scale it exhibits outstanding catalytic effects for a number of important chemical transformations.[1−3] The inertness of gold and many of its unusual properties derive from the strong relativistic effects[4] that stabilize the outer 6s shell and destabilize the 5d shell, inducing significant s−d hybridization. The structures of unsupported gold clusters provide the foundation for a mechanistic understanding of the catalytic and other unique properties of nanogold and have been intensely studied. Small gold cluster anions (Au_n^-) have been found to be planar up to 12 atoms[5] and are understood by the significant s−d hybridization.[6] In the intermediate size range, Au_{16} to Au_{18} have been found to form hollow cage clusters,[7] whereas Au_{20} forms a highly stable tetrahedral structure.[8] Larger gold clusters pose major challenges because of their structural diversity.[9−11] The largest bare Au cluster that has been well characterized experimentally is Au_{34}^-,[12,13] consisting of a core−shell structure with a 4-atom core and 30-atom shell. Despite significant theoretical efforts,[14−19] the structures of large bare gold clusters remain unresolved. An interesting set of large hollow gold cage clusters has been proposed,[20−24] but none has been confirmed experimentally.[25]

Here we focus on gold clusters with 55 to 64 atoms using photoelectron spectroscopy (PES) of size-selected anions and first principles calculations. These clusters with diameters larger than 1 nm belong to a critical size regime connecting small gold clusters to gold nanoparticles. The 55-atom clusters are of particular interest because they are a magic number in the Mackay icosahedral series. However, several calculations using empirical potentials have predicted that Au_{55} possesses an amorphous-like structure.[15−17,19] Indeed, a previous PES and theoretical study on coinage metal clusters has confirmed that Au_{55}^- is nonicosahedral, even though Cu_{55}^- and Ag_{55}^- are icosahedral as evidenced by their simple and well-structured PES spectra.[9] By combining well-resolved PES data and first principles calculations, we have obtained a systematic understanding about the structures and structural evolution from Au_{55}^- to Au_{64}^-. Both anions and neutral clusters are found to have similar structures, confirmed by the relatively sharp ground-state PES feature for each cluster. Although all clusters are found to possess low symmetry (C_1) (in particular, Au_{55}^- is highly distorted), clear core−shell type structures emerge from Au_{56}^- onward. Au_{56}^- and Au_{57}^- consist of
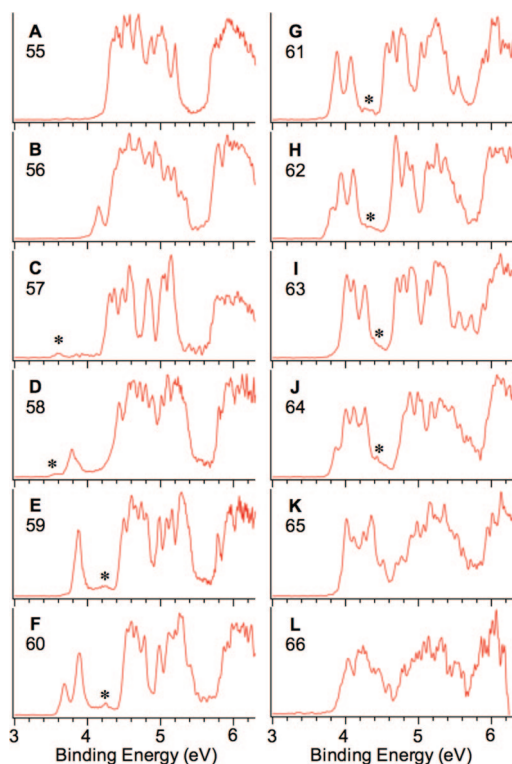
Figure 1. Photoelectron spectra of Au_n^- ($n = 55-66$) at 193 nm (6.424 eV). The weak feature indicated by the ∗ was likely due to contributions from a minor isomer.

a central atom and a 10-atom first shell with a 45- and 46-atom outer shell, respectively. Au_{58}^- is found to possess a central atom, an 11-atom first shell and a 46-atom outer shell. The 12-atom core of Au_{58}^- can be viewed as removing one apex atom from a distorted Au_{13} icosahedron. Remarkably, this cluster is found to be nearly spherical and structurally very robust: all larger clusters from Au_{59}^- to Au_{64}^- can be considered by adding extra atoms to square defects on the Au_{58}^- cluster surface. The origin of the nonicosahedral nature of Au_{55}^- and the low-symmetry structures of gold nanoclusters has been identified as due to the strong relativistic contractions of the cluster surface, analogous to reconstructions of bulk gold surfaces. The unique low-symmetry structures (which guarantee abundant supply of surface defect sites) uncovered for bare gold clusters in this critical size regime may hold the key to understanding the catalytic effects of gold nanoparticles.

Photoelectron Spectroscopy: Evidence for a Robust Au_{58}^- Cluster and Layered Growth from Au_{59}^- to Au_{64}^-. The PES experiment was carried out using a magnetic-bottle time-of-flight apparatus equipped with a laser vaporization cluster source at room temperature.[26] Negatively charged clusters were analyzed using a time-of-flight mass spectrometer and were mass-selected before photodetachment using the 193 nm (6.424 eV) radiation from an ArF excimer laser. The 193 nm spectra for Au_n^- ($n = 55-66$) are shown in Figure 1. These spectra are considerably better resolved than a previous survey

study by Taylor et al.[27] (The current spectra for Au_{55}^-, Au_{57}^-, and Au_{58}^- at room temperature are comparable to a recent study at 200 K condition.[9])

The PES spectra represent approximately the occupied electron density of states (DOS) of the negatively charged clusters. As pointed out by Taylor et al.,[27] the lower binding energy features from about 3.5 to 5.5 eV come primarily from the Au 6s states, whereas the congested PES features beyond 5.6 eV are mainly derived from the Au 5d band. Rich fine features were resolved in the low binding energy 6s band, providing electronic and structural information for the underlying clusters. The threshold peak, which characterizes detachment transition from the ground-state of the anion to that of the neutral cluster, is relatively sharp, suggesting that there is little structural change from the anion to the neutral. A clear even−odd effect was observed in the electron binding energies of the threshold peak, indicating that all the odd-sized cluster anions possess closed electron shells, whereas the even-sized cluster anions are open-shell. In other words, for neutral clusters the even-sized clusters possess closed-shell electron configurations with an energy gap between their highest occupied molecular orbital (HOMO) and their lowest unoccupied molecular orbital (LUMO). The weaker threshold peak in all the spectra of the even-sized clusters comes from detachment of the single electron in the LUMO [i.e., the singly occupied MO (SOMO) of the anion], and the observed energy gap represents the HOMO−LUMO gap of the neutral cluster. Au_{58} exhibits the largest HOMO−LUMO gap (0.65 eV) in this size range, because 58 valence electrons belong to a magic number in the jellium model representing a major electron shell closing.[28]

The most striking observation is in the size range from Au_{59}^- to Au_{64}^- (Figure 1E−J). The spectra of all these clusters display unprecedented similarities to that of Au_{58}^-: the effect of the additional atoms seems simply to contribute one valence electron, which successively fills up the LUMO or SOMO following the aufbau principle. For example, the spectrum of Au_{59}^- is almost identical to that of Au_{58}^-,[29] except that Au_{59}^- is closed shell with two electrons in its HOMO, as evidenced by the stronger intensity of its threshold peak at 3.88 eV (Figure 1E). The energy gap revealed in the Au_{59}^- spectrum between the first and second PES peaks is the same as that in Au_{58}^- and even the fine features in the 5d band around 5.9 eV are very similar in the two spectra, suggesting that the extra atom in Au_{59}^- is simply added to the surface of Au_{58}^- without inducing significant electronic and structural changes to the Au_{58}^- parent. In Au_{60}^-, the extra electron has to fill a new level because the HOMO of Au_{59}^- is completely filled with two electrons already, as evident by the new spectral feature at the threshold at 3.68 eV (Figure 1F). The second peak in the Au_{60}^- spectrum has an identical binding energy as the threshold peak of the Au_{59}^- spectrum

(3.88 eV) and the energy gap between the second peak and the third peak in the spectrum of Au_{60}^- is also identical to the energy gap observed in Au_{58}^- and Au_{59}^-, strongly suggesting that the extra atoms in Au_{60}^- induce very little perturbation to the electronic and atomic structures of the parent Au_{58}^-. In Au_{61}^-, the extra electron enters the SOMO of Au_{60}^-, producing two nearly equally intense peaks in the threshold region.

This electron filling pattern continues until Au_{64}^-, which possesses seven extra electrons beyond the shell closing at Au_{58}. These seven electrons yield three filled orbitals and a half-filled SOMO, as evident from the PES features of Au_{64}^- between 3.8 and 4.3 eV.[29] Beyond Au_{64}^-, such simple electronic filling pattern is no longer so obvious, as shown in the spectra of Au_{65}^- and Au_{66}^- (Figure 1K and L). It is conceivable that the Au_{58} core may be altered in the larger clusters with significant structural changes. To summarize, the electron-filling pattern from Au_{58}^- to Au_{64}^- revealed by the PES data provided several structural hints: (1) Au_{58}^- possesses a highly stable structure, (2) the extra atoms from Au_{59}^- to Au_{64}^- are added to the surface of Au_{58}^- without inducing major structural changes, and (3) there is no electronic degeneracy near the HOMO for Au_{58}^- to Au_{64}^-, that is, all these clusters are likely to have low symmetries.

Why Au_{55}^- Is Not Icosahedral: Relativistic Contraction of the Outer Layer in Analogy to Reconstruction of Bulk Gold Surfaces. What is this highly stable structure of Au_{58}^- and how do the clusters evolve from Au_{58}^- to Au_{64}^-? We carried out calculations based on the density functional theory with generalized gradient approximation (GGA) implemented in the VASP code.[30] It should be pointed out that these clusters are quite complex and extremely challenging computationally. However, the VASP code has been shown previously to be fairly efficient for treating gold clusters and yield reasonable results in comparison to other methods.[12,20,25] More importantly the PES spectra are quite unique in this size range, providing valuable structural hints as mentioned above. Both anions and neutral clusters were calculated and they were found to exhibit very similar structures, consistent with the sharp PES peaks. Our discussion and presentation will focus on the anions (Figures 2–6). Our structural search started from the 55-atom Au cluster, which has been shown to assume low-symmetry structures using various empirical potentials,[15–18] although its exact structure and why it is not icosahedral have not been resolved.

We first optimized Au_{55}^- without symmetry constraint starting from the I_h structure (Figure 2A). After an initial optimization the outer shell of the I_h-Au_{55}^- was observed immediately to change from A to B (Figure 2), in which three surface bonds were broken and a small "hole" appeared (Figure 2B: a second hole is also present at the back). Further optimization led to Figure
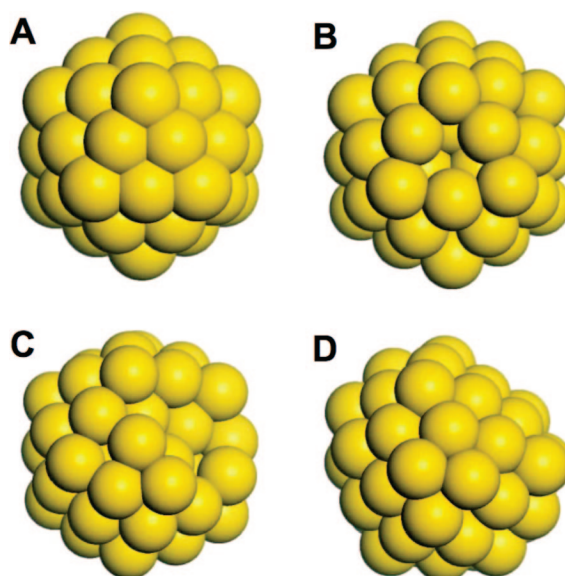
Figure 2. Structure evolution of Au_{55}^-. From the icosahedral Au_{55}^- (A), structural optimization reveals the breaking of surface bonds (B) due the outer shell contraction, the formation of surface holes (C), and finally the global minimum amorphous structure (D), in which several atoms from the first shell appear to move up to fill the surface holes.

2C, in which two small holes fused together to form a larger hole. This observation demonstrates clearly that Au_{55}^- cannot keep the I_h symmetry because of surface segregation resulting in shorter Au–Au distances. Interestingly, this behavior is analogous to reconstructions taking place on bulk Au surfaces.[31] It is well-known that the low-index surfaces of gold reconstruct. For example, the ideal Au(100) surface should have a square lattice, but experiments reveal that the top layer of this surface corresponds to a contracted hexagonal-closed-packed structure. A 20% area contraction is measured for Au and is shown to be entirely due to the relativistic effects.[31] Calculations by turning off the relativistic effect do not lead to the reconstruction, as is known for the corresponding Ag(100) surface.[31] For comparison we also performed similar calculations on Ag_{55}^- and found that it did keep the I_h symmetry after optimization, in agreement with previous conclusions that both Ag_{55}^- and Ag_{55}^+ possess the I_h structure.[9,32]

After further annealing, the final optimized structure of Au_{55}^- is shown in Figure 2D, which seems to adopt a less close-packed structure in the cluster interior (larger volume than the I_h structure) and is 1.65 eV more stable than the I_h structure. The center atom now has only about 8 nearest neighbors (Figure 4A) relative to 12 in the ideal I_h structure: several inner atoms have moved outward to fulfill the surface holes. This kind of reconstruction led to a highly disordered or amorphous-like structure for Au_{55}^-, as shown more clearly in the distance distributions of the outer atoms relative to the center atom (Figure 4A). The driving force underlying the structural distortions of Au_{55}^- from the ideal I_h structure is to optimize surface interactions at
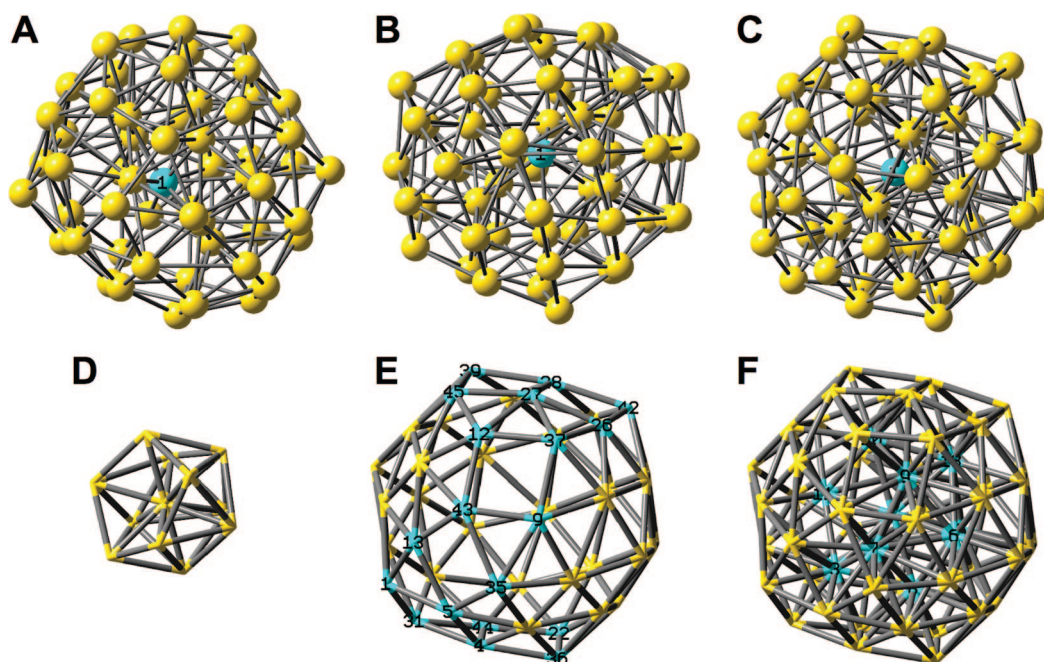
Figure 3. Optimized structures of (A) Au_{56}^-, (B) Au_{57}^-, and (C) Au_{58}^-, (D) the structure of the 12-atom core of Au_{58}^-, (E) the 46-atom outer shell of Au_{58}^-, where the surface square-defects are highlighted, and (F) the structure of Au_{58}^-, in which the inner core is highlighted.

the expense of the interior, entirely due to the relativistic effect analogous to the bulk surface reconstruction.[31] We found that in the optimized Au_{55}^- structure the surface atoms have much shorter bond length (2.83 Å) than that in an I_h-Au_{55}^- (2.91 Å). The DOS of this highly disordered Au_{55}^- (Figure 5A) agrees qualitatively with the experimental PES spectrum, whereas an I_h-Au_{55}^- would give a much simpler DOS spectrum.[9]

Figure 4. Plots of atomic distances from the center atom for the optimized structures of Au_n^- ($n = 55-64$). Two atomic shells are clearly revealed for $n = 56-64$.

Au_{56}^-, Au_{57}^-, and Au_{58}^-: Core−Shell Space-Filling Structures with "Bubbles". In Au_{55}^-, because of the finite cluster size several first shell atoms in the original I_h structure move outward to fulfill the surface holes created as a result of the relativistic contractions of the outer shell, resulting in a highly disordered structure (Figures 2D and 4A). To further understand the effects of the surface contractions, we optimized an I_h-Au_{55}^- with its 13-atom I_h core fixed, but allowed its surface atoms to relax. We found three surface holes are formed and the corresponding surface bond lengths are shortened to about 2.86 Å, compared to 2.91 Å in the ideal I_h structure. Subsequently, we added three atoms to fill the holes of the core-constrained Au_{55}^- and reoptimized the newly formed Au_{58}^- cluster. After the cluster was annealed, the final optimized structure (Figure 3C), which is 0.24 eV lower in total binding energy, has undergone some substantial structural rearrangement. This structure possesses no symmetry (C_1), but has a clear core−shell structure (Figure 4D). Interestingly, one of the first shell atoms has moved out to the outer shell, which has 46 atoms (Figure 3E). Its inner core, as shown in Figure 3D, becomes a distorted icosahedron with a missing apex atom. Despite its low symmetry, the structure of Au_{58}^- is in fact highly spherical: the ratio of its three principal axes is 1.0:1.0:1.0. The simulated DOS of this structure (Figure 5D) exhibits a large energy gap and is in good agreement with the experimental PES spectrum of Au_{58}^-. It is noteworthy that the HOMO−LUMO gap of Au_{58} is much larger than that in the corresponding Cu_{58} and Ag_{58} clusters[9] likely due to its highly spherical structure.
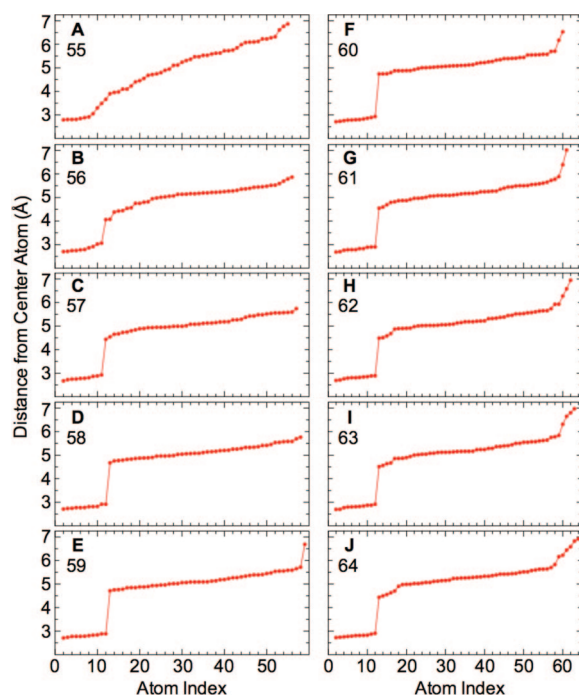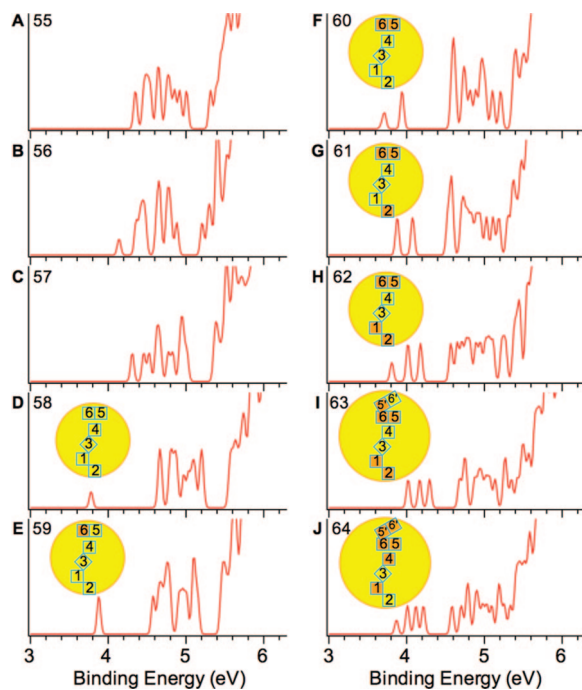
Figure 5. Simulated density of states for Au_n^- ($n = 55-64$). The Fermi level is aligned with the first photodetachment feature in each case. The inset in (D) is a structural model showing the six square-defect sites on the surface of Au_{58}^- indexed according to Figure 3E (1, $Au1-5-4-31$; 2, $Au4-36-22-44$; 3, $Au5-13-43-35$; 4, $Au9-37-12-43$; 5, $Au26-27-28-42$; 6, $Au27-28-39-45$). For $n = 59-64$, structural models for the atomic positions of the adatoms on the Au_{58}^- surface are shown. Note the appearance and occupation of two new defects (5′ and 6′) in (I) and (J).

We filled the holes of the core-constrained Au_{55}^- with one and two atoms and reoptimized the clusters to yield the final structures for Au_{56}^- (Figure 3A) and Au_{57}^- (Figure 3B), respectively. Both clusters have low symmetries (C_1), but with clear core–shell structures (Figure 4). The simulated DOS spectra for these two clusters (Figure 5) are in good agreement with the experimental PES spectra. In particular, the low binding energy part in the DOS spectrum of Au_{57}^- (Figure 5C) is almost in quantitative agreement with the experimental PES spectrum (Figure 1C). For Au_{56}^-, the observed HOMO–LUMO gap (Figure 1B) is well reproduced by the DOS spectrum (Figure 5B), but the observed PES spectrum seems to contain many more features than the DOS spectrum. This is because Au_{56}^- has a doublet ground-state with one unpaired electron in its SOMO. Photodetachment from Au_{56}^- can lead to both triplet and singlet final states, which cannot be accounted for in the DOS spectrum. The core of Au_{57}^- only contains 11 atoms and two of the inner shell atoms in the original icosahedral core have moved to fill the surface holes to create a 46-atom outer shell (Figure 4C), which is similar to that of Au_{58}^-. Similarly, in Au_{56}^- two inner shell atoms have also moved to the surface to give a 45-atom outer shell (Figure 4B), which is clearly less ordered than the outer shell of Au_{57}^-, but much more ordered than that of Au_{55}^-.

A major driving force in these clusters is to create a closer-packed surface layer because of the strong relativistic effects even at the expense of the inner core. This reconstruction produces voids or "bubbles" below the surface layer. For example, in Au_{58}^- there is a substantial void in the position of the missing first shell atom (If we move one surface atom to fill the bubble, the optimized structure is 0.5 eV higher in energy with a small pentagonal hole on the surface). Two voids exist in Au_{56}^- and Au_{57}^-, leading to slightly more disordered surface layers. In Au_{55}^-, three voids would have been created if three inner shell atoms were to move to the outer shell. Apparently, this is not sustainable and the surface appears collapsed, resulting in the highly disordered final structure for Au_{55}^-. The bubbles in these gold clusters, which are slightly smaller in size than the free-standing hollow golden cages of Au_{16}^- and Au_{17}^-,[7] are highly unusual. Their origin derives from the strong relativistic effects of gold to form a closer-packed outer layer. This phenomenon, which underlies the unusual low-symmetry structures for the gold nanoclusters, is analogous to the bulk gold surface, where the reconstructed closer-packed surface layer is incommensurate with the underlying substrate, but the energy gain due to the relativistic contraction in the surface layer is more than compensating for the energy loss due to the mismatch with the substrate.[31]

Au_{59}^- to Au_{64}^-: Layered Growth Based on a Robust Au_{58}^- Core. The PES data (Figure 1) suggest that Au_{58}^- is a uniquely stable cluster and the larger clusters up to Au_{64}^- appear to be formed by simply adding extra atoms to its surface without inducing significant structural and electronic changes. Remarkably, despite its nearly spherical structure the surface of Au_{58}^- contains six square-defect sites (Figure 3E), which provide ideal anchoring points for the adatoms. We put extra atoms to these defect sites successively and reoptimized the cluster structures from Au_{59}^- to Au_{64}^- and found that indeed the adatoms do not significantly change the parent Au_{58}^- structure (Figure 6). More importantly, the DOS spectra from these clusters (Figure 5E–J) can well reproduce the experimental observations.

For each cluster, we tested all the possible defect sites. For Au_{59}^-, there is a small energy difference among the six sites, but all six structures yield DOS spectra with a large gap between the first and second bands. The capping of site 6 gives the largest gap (Figure 5E); its structure is shown in Figure 6A. We also tested the structure by filling the bubble of Au_{58}^- with one atom; the resulting structure is higher in energy by 0.5 eV. For Au_{60}^-, we tested structures based on that of Au_{59}^- by adding an atom to the remaining five square defect sites. The DOS spectra for several low-lying structures are compared with the experimental spectrum in Supporting Information, Figure S1 for Au_{60}^-. It is found that the structure with sites 5 and 6 occupied yields a DOS spectrum (Figure 5F) in best
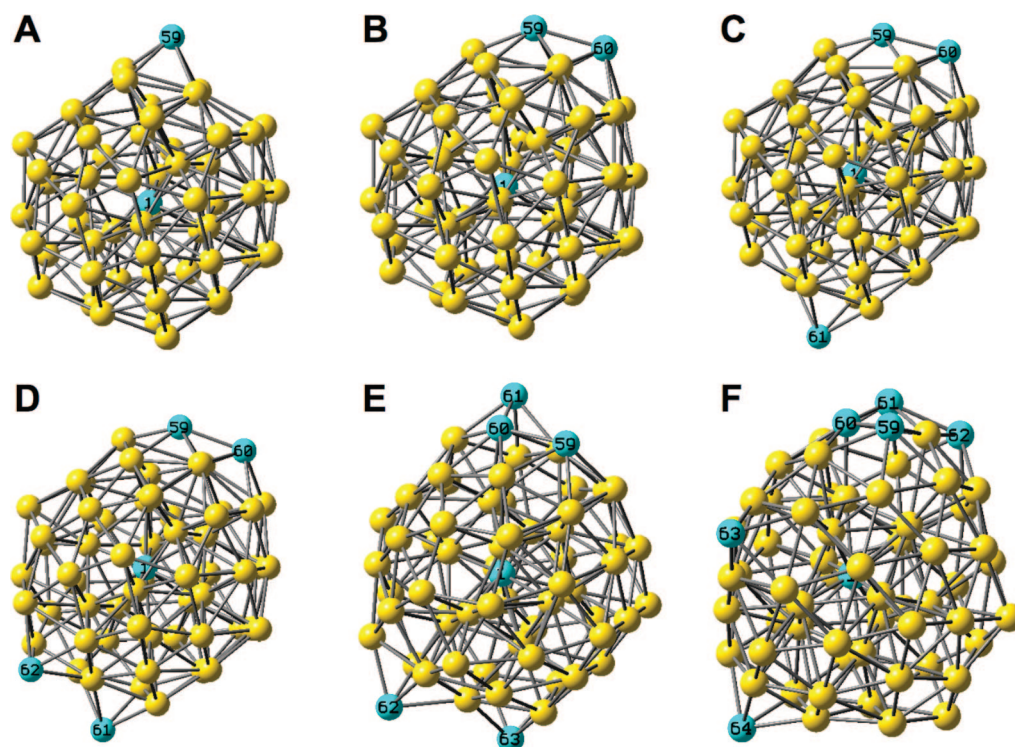
Figure 6. Optimized structures of Au_n^- ($n = 59-64$). The central atom and the adatoms are highlighted.

overall agreement with the PES spectrum. The DOS spectrum for the structure with sites 1 and 6 occupied is also consistent with the PES spectrum in term of the spacings in the first few peaks, but it is 0.26 eV higher in energy. Since sites 5 and 6 are adjacent to each other, it is energetically favorable to have them occupied first. For Au_{61}^- and Au_{62}^-, sites 2 and 1 are subsequently occupied (Figure 5G and H), yielding DOS spectra agreeing well with the experiment, in particular for the first few PES features in the low binding energy range.

Successive capping of sites 3 and 4 yielded stable structures for Au_{63}^- and Au_{64}^-, whose simulated DOS spectra exhibit similarities to the PES spectra, but the spacings among the first 3 or 4 bands appeared too close. We noted that as more atoms are added two new defect sites are created next to sites 5 and 6 (sites 5′ and 6′ in Figure 5I) owing to a slight reorganization of the surface layer of the parent Au_{58}^-. Occupation of these two new sites in Au_{63}^- and Au_{64}^- yields DOS spectra in better agreement with the experiment in term of the separations among the first 4 or 5 peaks, as shown in Figure 5 panels I and J, respectively. It is important to note that despite the small relaxation of the surface layer, the 12-atom core remains nearly identical to that in Au_{58}^- in all the surface-capping isomers from Au_{59}^- to Au_{64}^- (Figure 4E−J). It is conceivable that larger clusters beyond Au_{64}^- may continue to grow in a similar fashion. But more significant structural change may occur because the electronic states near the Fermi level begin to bunch up as revealed by the more congested PES spectra near the threshold region for Au_{65}^- and Au_{66}^- (Figure 1). Overall, the good agreement be-

tween the simulated DOS spectra and the experimental PES spectra, in particular for the clusters from Au_{58}^- to Au_{64}^- in the low binding energy range, lends considerable credence to the low-symmetry structures and growth pattern of gold nanoclusters in this critical size regime.

Implications for Nanogold Catalysis: Low-Symmetry and Abundant Supplies of Surface Defect Sites. Preparative-scale gold clusters passivated by ligands or surfactant have been found to often assume well-ordered structures.[33,34] The surface reconstructions imposed by the strong relativistic effects have been uncovered to result in low-symmetry structures for the naked gold nanoclusters. These uniquely low-symmetry structures may provide a key insight into understanding the catalytic effects of nanogold. Extensive research efforts have been carried out to elucidate the catalytic mechanisms of nanogold.[35] Small clusters with a few atoms have been shown to be catalytically active both in the gas phase and on oxide substrates.[36] Supported gold films with two monolayers of gold are found to be especially active.[37] All these model systems have one thing in common: they have plenty of low coordination sites, which are suggested to be critical for the enhanced catalytic effects of gold nanoparticles.[38,39] The low symmetry structures discovered here for gold nanoclusters in the 1−2 nm size regime guarantee abundant supplies of low coordination surface sites or defect sites, which may be the key for their catalytic activities. The low symmetry gold nanoclusters thus provide a critical structure−function relationship to understanding the mechanisms of nanogold. High symmetry structures

tend to have well-ordered surfaces and low coordination surface sites in such clusters decrease rapidly with increasing cluster size. It is conceivable that gold nanoparticles larger than 5 nm may transform into more bulklike structures or more ordered structures, thus becoming catalytically inactive.

METHODS

Photoelectron Spectroscopy. The experiment was carried out using a magnetic-bottle PES apparatus, which has been described in detail previously.[26] The Au_n^- cluster anions were produced by laser vaporization of a gold disk target with a helium carrier gas. The anions were extracted perpendicularly from the cluster beam and analyzed using time-of-flight mass spectrometry. The cluster of interest was mass-selected and decelerated before being photodetached by a 193 nm (6.424 eV) laser beam from an ArF excimer laser. The photoelectron time-of-flight spectra were converted to the electron kinetic energy spectra calibrated by the known spectrum of Au^-. The presented electron binding energy spectra were obtained by subtracting the kinetic energy spectra from the photon energy. The resolution of the magnetic-bottle PES apparatus was $\Delta E / E \approx 2.5\%$, that is, about 25 meV for 1 eV electrons.

Theoretical Methods. The theoretical calculations were done using density functional theory with generalized gradient approximation (GGA) implemented in the VASP code. The VASP code is an efficient simulated-annealing method, which allows local minima to be readily identified.[30] In the calculations only the valence electrons ($5d^{10}6s^1$) were treated explicitly and their interactions with the ionic cores were described by the PAW pseudopotentials with scalar relativistic effects included.[40] The wave functions were expanded in plane waves with an energy cutoff ~230 eV. A simple cubic cell with 30 Å edge length was used with periodic boundary conditions, and the Γ point approximation was used for Brillouin zone sampling. The accuracy of the present calculation was checked by calculating the bond length of Au_2 dimer and the lattice constant of bulk gold. The present PAW pseudopotential method can correctly predict the binding properties of the dimer and the bulk. Simulated annealing and conjugate gradient method were used to optimize the global structures. We carried out extensive searches for the global minima for Au_n^- ($n = 55-58$). For $n > 58$, the structural search was guided by the experimental hint such that additional atoms were added to the surface of Au_{58}^-, followed by full structural optimizations. All structures were optimized by the conjugated-gradient method with a force convergence of 1.0×10^{-3} eV Å^{-1}. Density of state spectra were simulated to compare with the experimental PES spectra. The DOS spectra were simulated by fitting gaussians (0.05 eV width) to all occupied electronic states below the Fermi level. The Fermi level was aligned with the first PES feature to facilitate the comparison.

Supporting Information Available: Figure S1: Simulated DOS spectra for several low-lying structures and their relative energies for Au_{60}^- in comparison with the experimental PES spectrum. This material is available free of charge *via* the Internet at http://pubs.acs.org.

REFERENCES AND NOTES

1. Haruta, M. Size- and Support-Dependency in the Catalysis of Gold. *Catal. Today* **1997**, *36*, 153–166.
2. Hayashi, T.; Tanaka, K.; Haruta, M. Selective Vapor-Phase Epoxidation of Propylene over Au/TiO$_2$ Catalysts in the Presence of Oxygen and Hydrogen. *J. Catal.* **1998**, *178*, 566–575.
3. Hughes, M. D.; Xu, Y.-J.; Jenkins, P.; McMorn, P.; Landon, P.; Enache, D. I.; Carley, A. F.; Attard, G. A.; Hutchings, G. J.; King, F.; Stitt, E. H.; Johnston, P.; Griffin, K.; Kiely, C. J. Tunable Gold Catalysts for Selective Hydrocarbon Oxidation under Mild Conditions. *Nature* **2005**, *437*, 1132–1135.
4. Pyykkö, P. Relativistic Effects in Structural Chemistry. *Chem. Rev.* **1988**, *88*, 563–594.
5. Furche, F.; Ahlrichs, R.; Weis, P.; Jacob, C.; Gilb, S.; Bierweller, T.; Kappes, M. M. The Structures of Small Gold Cluster Anions as Determined by a Combination of Ion Mobility Measurements and Density Functional Calculations. *J. Chem. Phys.* **2002**, *117*, 6982–6990.
6. Häkkinen, H.; Moseler, M.; Landman, U. Bonding in Cu, Ag, and Au Clusters: Relativistic Effects, Trends, and Surprises. *Phys. Rev. Lett.* **2002**, *89*, 033401.
7. Bulusu, S.; Li, X.; Wang, L. S.; Zeng, X. C. Evidence of Hollow Golden Cages. *Proc. Natl. Acad. Sci. U.S.A.* **2006**, *103*, 8326–8330.
8. Li, J.; Li, X.; Zhai, H. J.; Wang, L. S. Au$_{20}$: A Tetrahedral Cluster. *Science* **2003**, *299*, 864–867.
9. Häkkinen, H.; Moseler, M.; Kostko, O; Morgner, N.; Hoffmann, M. A.; Issendorff, B. V. Symmetry and Electronic Structure of Noble-Metal Nanoparticles and the Role of Relativity. *Phys. Rev. Lett.* **2003**, *93*, 093401.
10. Xing, X. P.; Yoon, B.; Landman, U.; Parks, J. H. Structural Evolution of Au Nanoclusters: From Planar to Cage to Tubular Motifs. *Phys. Rev. B* **2006**, *74*, 165423.
11. Yoon, B.; Koskinen, P.; Huber, B.; Kostko, B.; Issendorff, B. v.; Häkkinen, H; Moseler, M.; Landman, U. Size-Dependent Structural Evolution and Chemical Reactivity of Gold Clusters. *ChemPhysChem* **2007**, *8*, 157–161.
12. Gu, X.; Bulusu, S.; Li, X.; Zeng, X. C.; Li, J.; Gong, X. G.; Wang, L. S. Au$_{34}^-$: A Fluxional Core-Shell Cluster. *J. Phys. Chem. C* **2007**, *111*, 8228–8232.
13. Lechtken, A.; Schoos, D.; Stairs, J. R.; Blom, M. N.; Furche, F.; Morgner, N.; Kostko, O.; Issendorff, B. V.; Kappe, M. M. Au$_{34}^-$: A Chiral Gold Cluster? *Angew. Chem., Int. Ed.* **2007**, *46*, 2944–2948.
14. Häberlen, O. D.; Chung, S. C.; Stener, M.; Rosch, N. From Clusters to Bulk: A Relativistic Density Functional Investigation on a Series of Gold Clusters Au$_n$ $n = 6$,. ., 147. *J. Chem. Phys.* **2007**, *106*, 5189–5201.
15. Doye, J. P. K.; Wales, D. J. Global Minima for Transition Metal Clusters Described by Sutton-Chen Potentials. *New J. Chem.* **1998**, *22*, 733–744.
16. Garzón, I. L.; Michaelian, M.; Beltrán, M. R.; Posada-Amarillas, A.; Ordejón, P.; Artacho, E.; Sánchez-Portal, D. Soler, Lowest Energy Structures of Gold Nanoclusters. *Phys. Rev. Lett.* **1998**, *81*, 1600–1603.
17. Michaelian, K.; Rendon, N.; Garzon, I. L. Structure and Energetics of Ni, Ag, and Au Nanoclusters. *Phys. Rev. B* **1999**, *60*, 2000–2010.
18. Darby, S.; Mortimer-Jones, T. V.; Johnston, R. L.; Roberts, C. Theoretical Study of Cu-Au Nanoalloy Clusters Using a Genetic Algorithm. *J. Chem. Phys.* **2002**, *116*, 1536–1550.
19. Xiao, L.; Tollberg, B.; Hu, X. K.; Wang, L. C. Structural Study of Gold Clusters. *J. Chem. Phys.* **2006**, *124*, 114309.
20. Gu, X.; Ji, M.; Wei, S. H.; Gong, X. G. Au$_N$ Clusters ($N = 32,33,34,35$): Cagelike Structures of Pure Metal Atoms. *Phys. Rev. B* **2004**, *70*, 205401.
21. Johansson, M. P.; Sundholm, D.; Vaara, J. Au$_{32}$: A 24-Carat Golden Fullerene. *Angew. Chem., Int. Ed.* **2004**, *43*, 2678–2681.

22. Gao, Y.; Zeng, X. C. Au_{42}: An Alternative Icosahedral Golden Fullerene Cage. *J. Am. Chem. Soc.* **2005**, *127*, 3698–3699.

23. Wang, J.; Jellinek, J.; Zhao, J.; Chen, Z.; King, R. B.; Schleyer, P. v. R. Hollow Cages *versus* Space-Filling Structures for Medium-Sized Gold Clusters: the Spherical Aromaticity of the Au_{50} Cage. *J. Phys. Chem. A* **2005**, *109*, 9265–9269.

24. Karttunnen, A. J.; Linnolahti, M.; Pakkanen, T.; Pyykkö, P. Icosahedral Au_{72}: A Predicted Chiral and Spherically Aromatic Golden Fullerene. *Chem. Commun.* **2008**, 465–467.

25. Ji, M.; Gu, X.; Li, X.; Gong, X. G.; Li, J.; Wang, L. S. Experimental and Theoretical Investigation of the Electronic and Geometrical Structures of the Au_{32} Cluster. *Angew. Chem. Intl. Ed.* **2005**, *44*, 7119–7123.

26. Wang, L. S.; Cheng, H. S.; Fan, J. W. Photoelectron Spectroscopy of Size-Selected Transition-Metal Clusters—$Fe_n^- \ n = 3{-}24$. *J. Chem. Phys.* **1995**, *102*, 9480–9493.

27. Taylor, K. J.; Pettiettehall, C. L.; Cheshnovsky, O.; Smalley, R. E. Ultraviolet Photoelectron Spectra of Coinage Metal Clusters. *J. Chem. Phys.* **1992**, *96*, 3319–3329.

28. de Heer, W. A. The Physics of Simple Metal Clusters - Experimental Aspects and Simple-Models. *Rev. Mod. Phys.* **1993**, *65*, 611–676.

29. The very weak signals in the energy gap region around 4.2 eV in the spectrum of Au_{59}^- (labeled with ∗) was very likely due to the presence of a minor isomer. Similar weak signals were discernible in the spectrum of Au_{60}^- to Au_{64}^-, as well as in the very low binding energy side of Au_{57}^- and Au_{58}^-. Similar weak features were also observed previously for Au_{20}^- under conditions when hotter clusters were produced (see ref 27).

30. Kresse, G.; Furthmuller, J. Efficient Iterative Schemes for Ab Initio Total-Energy Calculations Using a Plane-Wave Basis Set. *Phys. Rev. B* **1996**, *54*, 11169–11186.

31. Takeuchi, N.; Chan, C. T.; Ho, K. M. Reconstruction of the (100) Surfaces of Au and Ag. *Phys. Rev. B* **1991**, *43*, 14363–14370.

32. Schooss, D.; Blom, M. N.; Parks, J. H.; Issendorff, B. V.; Haberland, H.; Kappes, M. M. The Structures of Ag_{55}^+ and Ag_{55}^-: Trapped Ion Electron Diffraction and Density Functional Theory. *Nano Lett.* **2005**, *5*, 1972–1977.

33. Whetten, R. L.; Khoury, J. T.; Alvarez, M. M.; Murthy, S.; Vezmar, I.; Wang, Z. L.; Stephens, P. W.; Cleveland, C. L.; Luedtke, W. D.; Landman, U. Nanocrystal Gold Molecules. *Adv. Mater.* **1996**, *8*, 428–433.

34. Jadzinsky, P. D.; Calero, G.; Ackerson, C. J.; Bushnell, D. A.; Kornberg, R. D. Structure of a Thiol Monolayer-Protected Gold Nanoparticle at 1.1 Angstrom Resolution. *Science* **2007**, *318*, 430–433.

35. Chen, M.; Cai, Y.; Yan, Z.; Goodman, D. W. On the Origin of the Unique Properties of Supported Au Nanoparticles. *J. Am. Chem. Soc.* **2006**, *128*, 6341–6346.

36. Yoon, B.; Hakkinen, H.; Landman, U.; Worz, A. S.; Antonietti, J.-M.; Abbet, S.; Judai, K.; Heiz, U. Charging Effects on Bonding and Catalyzed Oxidation of CO on Au_8 Clusters on MgO. *Science* **2005**, *307*, 403–407.

37. Chen, M. S.; Goodman, D. W. The Structure of Catalytically Active Gold on Titania. *Science* **2004**, *306*, 252–255.

38. Lopez, N.; Nørskov, K. Catalytic CO Oxidation by a Gold Nanoparticle: A Density Functional Study. *J. Am. Chem. Soc.* **2002**, *124*, 11262–11263.

39. Molina, L. M.; Hammer, B. Some Recent Theoretical Advances in the Understanding of the Catalytic Activity of Au. *App. Catal. A* **2005**, *291*, 21–31.

40. Kresse, G.; Joubert, D. From Ultrasoft Pseudopotentials to the Projector Augmented-Wave Method. *Phys. Rev. B* **1999**, *59*, 1758–1775.